NACA

RESEARCH MEMORANDUM

LANGLEY 9-INCH SUPERSONIC TUNNEL TESTS OF SEVERAL MODIFICATIONS OF A SUPERSONIC MISSILE HAVING TANDEM CRUCIFORM LIFTING SURFACES

THREE-COMPONENT DATA RESULTS OF MODELS HAVING RATIOS OF WING SPAN TO TAIL SPAN LESS THAN 1

By Robert W. Rainey

Langley Aeronautical Laboratory
Langley Field, Va.

NATIONAL ADVISORY COMMITTEE
FOR AERONAUTICS

WASHINGTON
March 7, 1951

NATIONAL ADVISORY COMMITTEE FOR AERONAUTICS

RESEARCH MEMORANDUM

LANGLEY 9-INCH SUPERSONIC TUNNEL TESTS OF SEVERAL MODIFICATIONS OF A SUPERSONIC MISSILE HAVING TANDEM CRUCIFORM LIFTING SURFACES

THREE-COMPONENT DATA RESULTS OF MODELS HAVING RATIOS OF WING SPAN TO TAIL SPAN LESS THAN 1

By Robert W. Rainey

SUMMARY

The lift, drag, and pitching-moment measurements from tests made in the Langley 9-inch supersonic tunnel of four missile configurations having wing-tail-span ratios less than 1 are presented. These configurations incorporated changes to wing and tail plan form and wing-tail-span ratios. Tests of the four complete missiles and their elements and combinations of elements at 0° and 45° roll angle were made at a Mach number of 1.93 and a Reynolds number of 0.27×10^6 based on the maximum body diameter or 3.08×10^6 based on body length. Tests of one missile and some of its elements and combinations of elements were made at Mach numbers of 1.62 and 2.40. The angle-of-attack range of these tests was from -5° to 15°. These data show the effects of wing-tail interference on the static longitudinal stability of these missile configurations.

INTRODUCTION

The lift, drag, and pitching-moment characteristics of a "basic" missile and several modified versions of the basic missile were presented in reference 1; the modifications were in body length, interdigitation angle, and wing plan form, and all configurations had equal-span wings and tails. In reference 2 were presented the three-component measurements and some static rolling-moment measurements of several modified versions of the basic configuration; these modifications included

changes in wing and tail plan forms of configurations having wing-tail-span ratios equal to and less than 1 as well as changes in interdigitation angle, nose shape, and body length.

In the present paper are presented three-component measurements of four more modified missiles with tandem, cruciform, low-aspect-ratio lifting surfaces and with wing-tail-span ratios less than 1. Of special interest is the configuration with three tandem lifting surfaces which was devised as a means of reducing the variation in static margin throughout the moderate angle-of-attack range. The data presented included the lift, drag, and pitching-moment characteristics of all four modified missiles and their components at a Mach number of 1.93 and of one of the modified missiles and some of its components at Mach numbers of 1.62 and 2.40 and corresponding Reynolds numbers of 0.362×10^6 and 0.262×10^6 per inch. With these data it is possible to obtain the characteristics of one component in the presence of another or others. In order to expedite publication of these data, no analyses of results are presented.

SYMBOLS

S	maximum body cross-sectional area
d	maximum body diameter
C_D	drag coefficient $\left(\frac{\text{Drag}}{qS}\right)$
C_L	lift coefficient $\left(\frac{\text{Lift}}{qS}\right)$
C_m	pitching-moment coefficient, moments taken about center of gravity indicated in figure 1 $\left(\frac{\text{Pitching moment}}{qSd}\right)$
q	dynamic pressure $\left(\frac{\rho V^2}{2}\right)$
α	angle of attack
ϕ	angle of roll of model relative to angle-of-attack plane, positive when model, viewed from rear, is rotated clockwise ($\phi = 0^\circ$ when opposite tail panels are in angle-of-attack plane)

[redacted]

θ angle between a plane through opposite tail panels and a plane through opposite wing panels, positive when wings are rotated clockwise with respect to tails, when the model is viewed from rear. The angle θ is always less than 90°, and its value appears as the superscript for W in the model configuration designations. When θ values are indicated for BW configurations, the subtracted tail is assumed to be present at $\phi = 0^{\circ}$.

B configuration of body

BT configuration of body and tails

BW configuration of body and wings

BWT configuration of body, wings, and tails

Subscripts:

T body has internal taper at stern

Numerical subscripts refer to the particular body, wing, or tail plan form (see fig. 1)

Superscripts:

Numerical superscript for W gives value of θ. (See definition of θ.)

APPARATUS AND TEST PROCEDURE

Wind Tunnel

All tests were conducted in the Langley 9-inch supersonic tunnel which is a continuous-operation closed-circuit type in which the stream pressure, temperature, and humidity conditions can be controlled and regulated. Different test Mach numbers are provided by interchanging nozzle blocks which form test sections approximately 9 inches square. Throughout the present tests, the moisture content in the tunnel was kept sufficiently low so that the effects of condensation in the supersonic nozzle were negligible. Eleven fine mesh turbulence-damping screens are provided in the relatively large area settling chamber just ahead of the supersonic nozzle. A schlieren optical system is provided for qualitative visual-flow observations.

[redacted]

Test Setup and Models

A schematic drawing of the model installation in the tunnel is shown in reference 1 with a description of the test setup. For the present tests, dimensions and designations of the various models used are given in figure 1 with the exception of B_{2_T} and $B_{4_T}W_1^0$ which were given in reference 1. Models were found generally to be accurate to within ±0.002 inch of the dimensions shown. The various wings and tails of the configurations could be changed, located differently with respect to each other on the body, or omitted entirely. Body lengths could be changed by inserting sections in or removing sections from the cylindrical portion. Also, nose shapes could be changed by a simple interchange of parts. All models tested had an internal taper at the stern of the body and the elevators soldered fixed to the tail panels (see reference 1). All of the elements and combinations of elements of the models are listed in the index of figures. The body-alone tests reported on were made by use of "solid" models whose surfaces were relatively free of waviness and protuberances.

PRECISION OF DATA

For all the test Mach numbers, pressure surveys throughout the test section have shown the stream to be uniform within a maximum variation in Mach number of ±0.01. Less detailed angle surveys have indicated negligible flow deviations and, also, from past experience, both zero moment and zero lift are generally realized for symmetrical configurations at zero angle of attack. These points are brought out to emphasize the fact that, for the present tests when an unexpected moment or lift appears at zero angle of attack, several possibilities exist; namely, the configuration is asymmetrical, the flow about the symmetrical configuration is asymmetrical, and/or an extraneous force appears as a result of the flow around the support system or windshield. For the present tests, the most likely reason for an extraneous moment or lift at zero angle of attack is a misalined (other than zero angle with respect to the body axis) wing or tail panel. Measurements of the various wings and tails indicated that inadvertent incidences are present which contributed to the various lifts and moments evident at zero angle of attack.

All the lift, drag, and pitching moment were measured by means of self-balancing mechanical scales. A conservative estimate of the maximum probable errors in these measurements is given in the following table:

[redacted]

Coefficient \ Mach number	1.62	1.93	2.40
C_L	±0.001	±0.001	±0.001
C_D	±.003	±.003	±.004
C_m	±.013	±.014	±.020

Reference to the data will show that these errors in the forces and moments are probably very small as compared with the scatter about a mean curve or displacement of a mean curve arising from other errors.

Angles of attack with respect to each other in a given run are accurate to within ±0.01°. The errors in initially referencing the body axis parallel to the air stream may be up to 0.03°.

PRESENTATION OF DATA

The lift, drag, and pitching-moment data are presented in figures 2 to 18. An index precedes the figures in which the figures are listed in order of presentation. The figures are grouped according to Mach number; for each Mach number, the data are approximately in the order of the model build-up; that is, first, body alone, then, body and wing, and so forth. In order to complete the data necessary to assess the configuration $B_{4_T}W_1^{45}T_1$ (see reference 2), the results of tests of $B_{4_T}W_1^{0}$ are presented in the present paper. Examination of the index of figures will show that, at a Mach number of 1.62, the component or breakdown tests for the configuration $B_{4_T}W_{11}^{45}T_7$ are incomplete. The configurations $B_{4_T}T_7$ at 0° roll angle $B_{4_T}W_{11}^{45}$ at 0° and 45° roll angle were not tested because of difficulties involving the balance system and, therefore, are not reported herein.

Included in the present paper are the results of solid body-alone tests with and without transition induced about the body (see figs. 2, 13, and 16). As in the previous body-alone tests reported on in reference 2, transition was induced by transition strips around the

[redacted]

body in the region where the wings were installed. Each ring was composed of fine salt crystals sparsely distributed in a single layer over a width of about 1/8 inch and a thickness of about 0.013 inch (1.6 percent diameter). These body-alone tests complete those needed to make a more complete analysis of the interference effects between components. A very brief discussion of the use of "solid" body models and tests with and without transition induced about the body is given in reference 2 under the section entitled "Presentation of Data, Body-Alone Tests".

An extension to these tests was made by determining the effects of transition on a body-tail configuration. The transition strip around the body was similar to those mentioned previously in the body-alone tests and was located in the region normally occupied by the wings. As indicated in figure 14, the effects of transition on the lift and pitching-moment characteristics of this body-tail configuration were negligible.

It is of interest to compare the characteristics of the rather unusual configuration $B_{4_T}W_{11}{}^{0}W_8{}^{45}T_7$ with those of $B_{4_T}W_{11}{}^{0}T_7$. This unusual configuration consisted of $B_{4_T}W_{11}{}^{0}T_7$ with the wing $W_8{}^{45}$ installed at about the center-of-gravity location (see fig. 1). The configuration $B_{4_T}W_{11}{}^{0}W_8{}^{45}T_7$ was tried in an effort to reduce the rearward center-of-pressure travel as the angle of attack of $B_{4_T}W_{11}{}^{0}T_7$ was increased. The insertion of $W_8{}^{45}$ provided an additional vortex system within the region occupied by T_7 at moderate angles of attack, and it was hoped that the additional downwash in the region of T_7 would be sufficient to reduce the tail lift somewhat and result in less rearward travel of the center of pressure. Also, the wing $W_8{}^{45}$ was installed at about the center of gravity so that the effects of its lift on the center-of-pressure location would be small.

In order to assess $B_{4_T}W_{11}{}^{0}W_8{}^{45}T_7$, its characteristics should be compared to those of $B_{4_T}W_{11}{}^{0}T_7$ (compare figs. 10 and 12). It can be seen that the addition of $W_8{}^{45}$ caused a large change in C_{m_α} in the low angle-of-attack range which resulted in the center-of-pressure location being ahead of its previous location. At the moderate and higher angles of attack the addition of $W_8{}^{45}$ resulted in the magnitudes

[redacted]

of lift and pitching moment becoming more nearly equal at both roll angles and of such magnitudes that the center-of-pressure travels were of the order of two-thirds those of $B_{\mu_T} W_{11}{}^{OT}{}_{7}$.

Langley Aeronautical Laboratory
National Advisory Committee For Aeronautics
Langley Field, Va.

REFERENCES

1. Rainey, Robert W.: Langley 9-Inch Supersonic Tunnel Tests of Several Modifications of a Supersonic Missile Having Tandem Cruciform Lifting Surfaces. Three-Component Data Results of Models Having Ratios of Wing Span to Tail Span Equal to 1. NACA RM L9L30, 1951.

2. Rainey, Robert W.: Langley 9-Inch Supersonic Tunnel Tests of Several Modifications of a Supersonic Missile Having Tandem Cruciform Lifting Surfaces. Three-Component Data Results of Models Having Ratios of Wing Span to Tail Span Equal to and Less than 1 and Some Static Rolling-Moment Data. NACA RM L50G07, 1951.

INDEX OF FIGURES

Figure	Mach number	Figure legends
1	----	Model dimensions and center-of-gravity location
2	1.93	Basic solid body characteristics with transition, B_{2_T} $W_1{}^\circ$ increments on B_{4_T} at roll angles
3	1.93	$W_{10}{}^\circ$ increments on B_{4_T} at roll angles $W_{11}{}^\circ$ increments on B_{4_T} at roll angles
4	1.93	$W_{13}{}^\circ$ increments on B_{4_T} at roll angles $W_{11}{}^\circ W_8{}^{45}$ increments on B_{4_T} at roll angles
5	1.93	T_7 increments on B_{4_T} at roll angles
6	1.93	$B_{4_T} W_{10}{}^\circ T_5$ at roll angles
7	1.93	$B_{4_T} W_{10}{}^{45} T_5$ at roll angles
8	1.93	$B_{4_T} W_{13}{}^\circ T_5$ at roll angles
9	1.93	$B_{4_T} W_{13}{}^{45} T_5$ at roll angles
10	1.93	$B_{4_T} W_{11}{}^\circ T_7$ at roll angles
11	1.93	$B_{4_T} W_{11}{}^{45} T_7$ at roll angles
12	1.93	$B_{4_T} W_{11}{}^\circ W_8{}^{45} T_7$ at roll angles
13	1.62	Effects of transition on basic solid body characteristics, B_{4_T}

[redacted]

INDEX OF FIGURES - Concluded

Figure	Mach number	Figure legends
14	1.62	T_7 increments on B_{4_T} at a roll angle of 45°
15	1.62	$B_{4_T} W_{11}{}^{45}T_7$ at roll angles
16	2.40	Effects of transition on basic solid body characteristics, B_{4_T} $W_{11}{}^{45}$ increments on B_{4_T} at roll angles
17	2.40	T_7 increments on B_{4_T} at roll angles
18	2.40	$B_{4_T} W_{11}{}^{45}T_7$ at roll angles

[redacted]

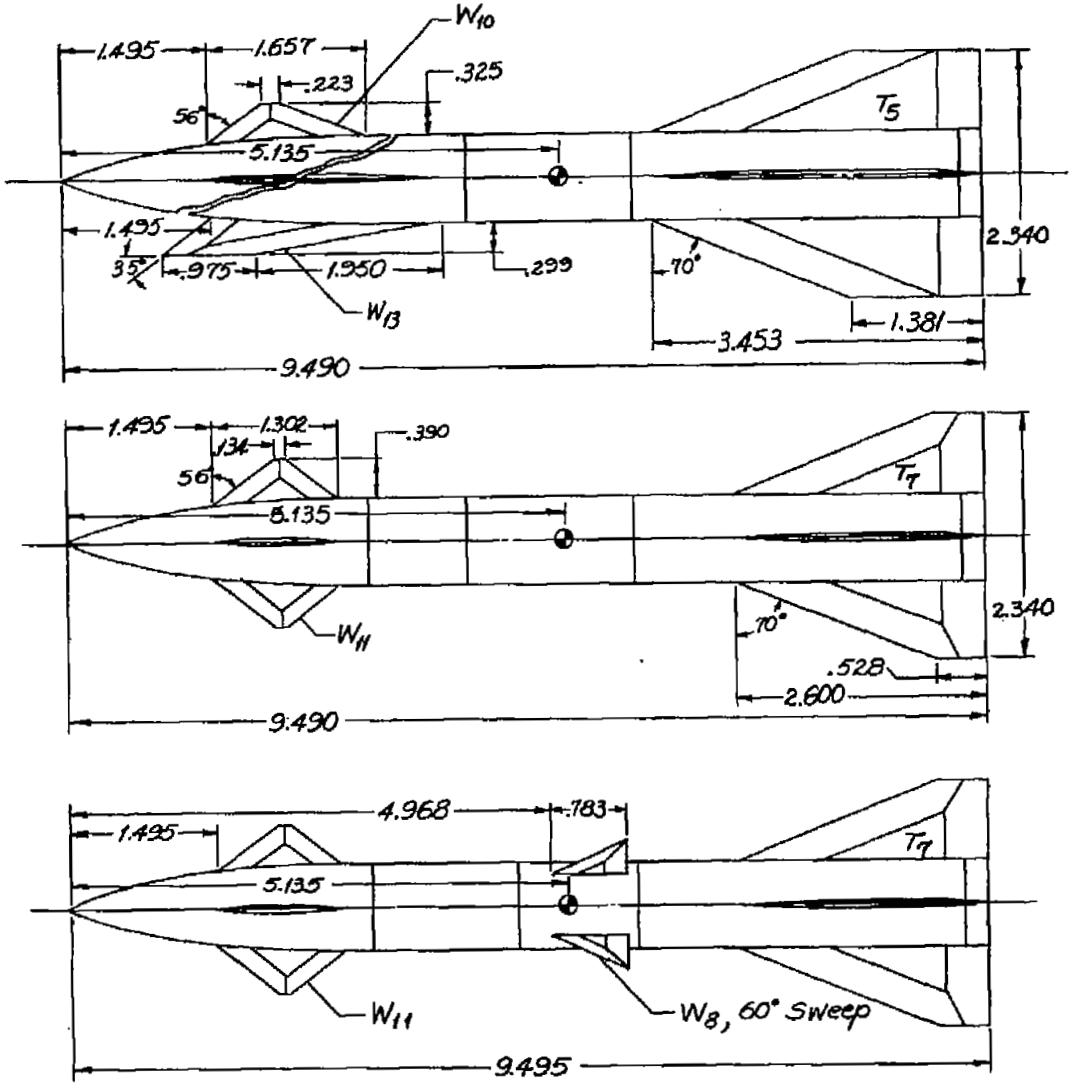

Surface	$(t/c)_{root}$	$(t/c)_{tip}$
T_5	.018	.045
T_7	.024	.087
W_8	.079	---
W_{10}	.037	.046
W_{11}	.048	.119
W_{13}	.021	.020

Figure 1.- Model dimensions and center-of-gravity location.

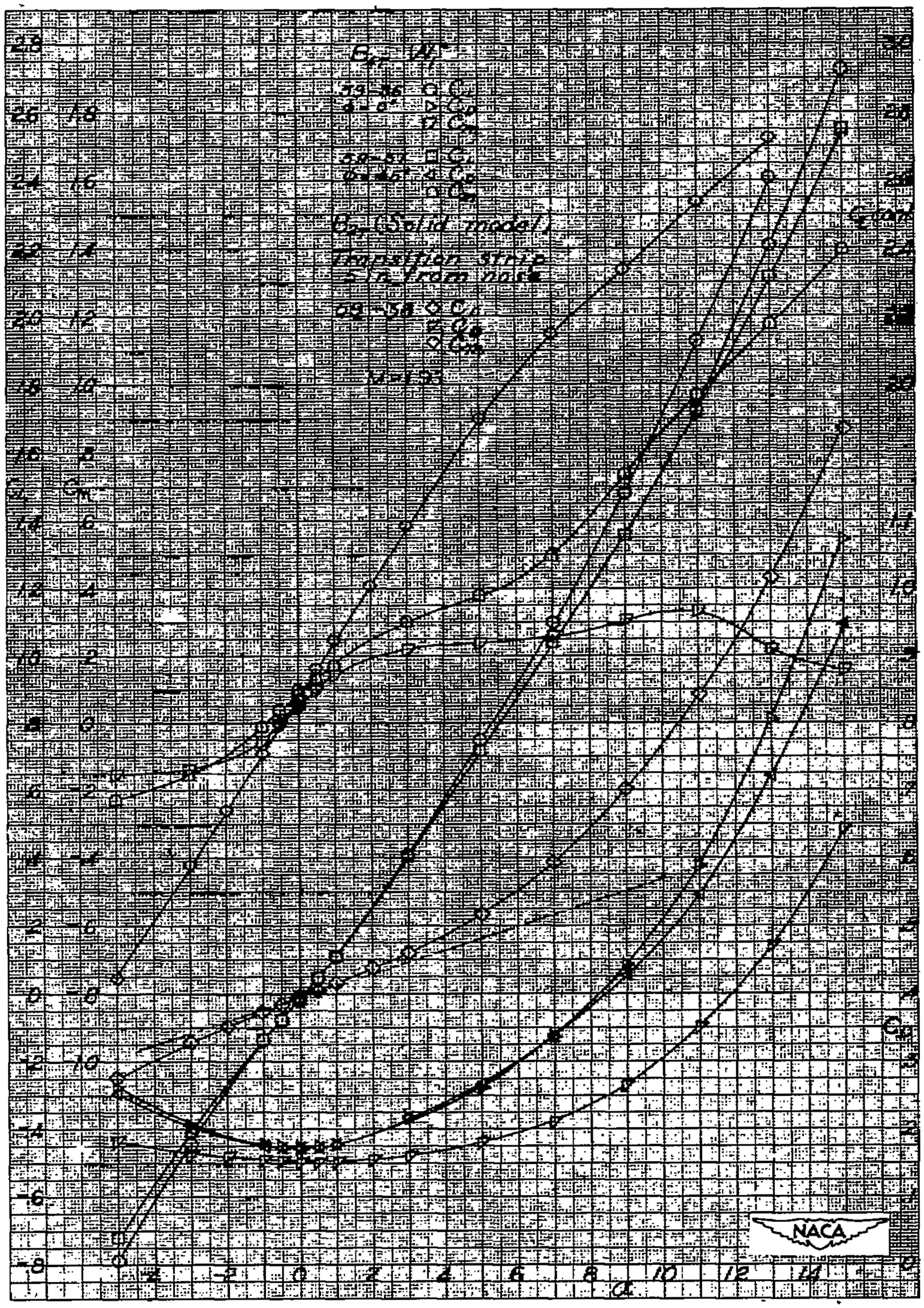

Figure 2.- M = 1.93: Basic solid body characteristics with transition, B_{2_T}; $W_1{}^0$ increments on B_{4_T} at roll angles of 0° and 45°.

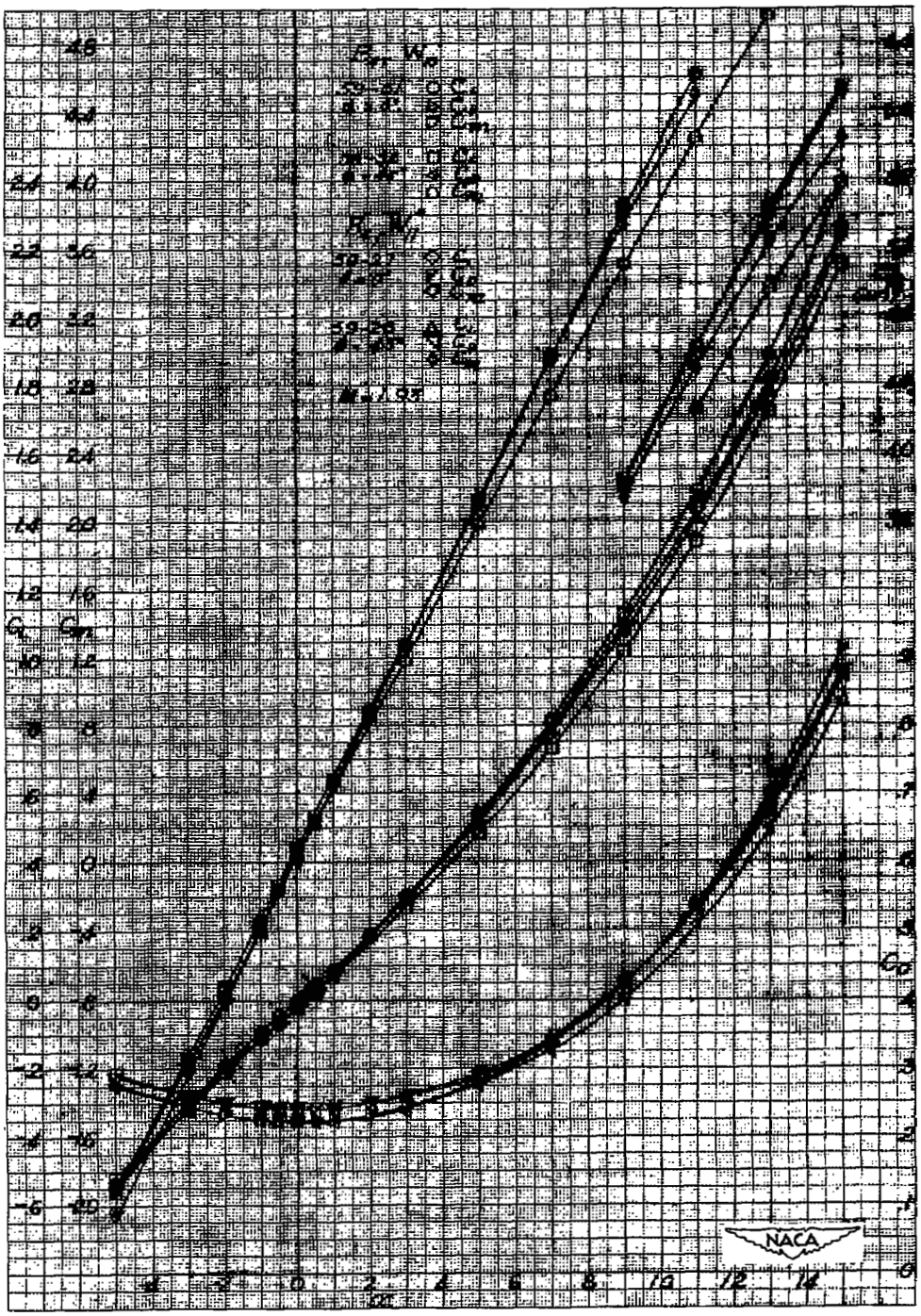

Figure 3.- M = 1.93: $W_{10}{}^{0}$ and $W_{11}{}^{0}$ increments on Bl_{4_T} at roll angles of 0° and 45°.

[redacted]

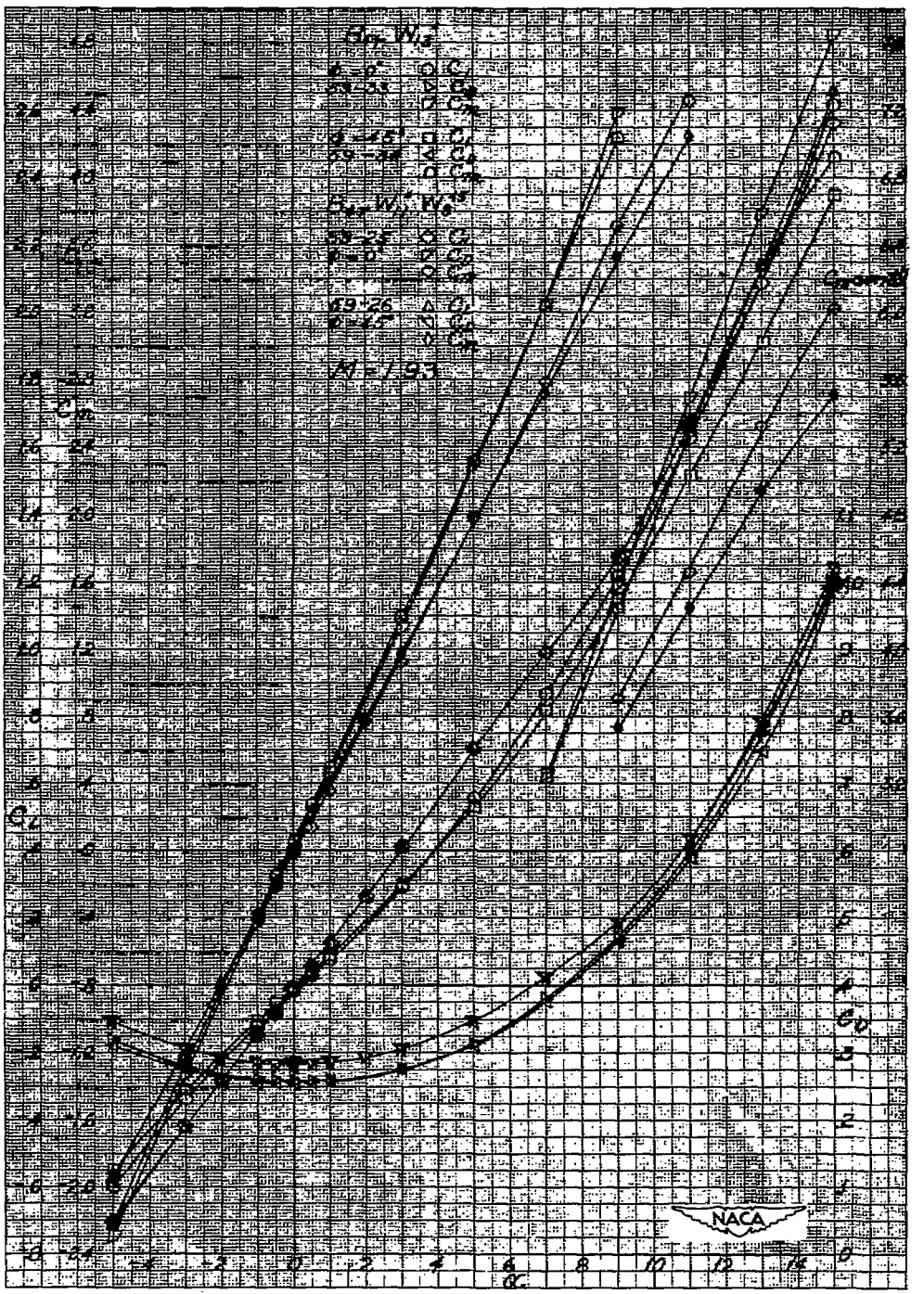

Figure 4.- M = 1.93: $W_{13}{}^{0}$ and $W_{11}{}^{0}W_{8}{}^{45}$ increments on $B1_{T}$ at roll angles of 0° and 45°.

[redacted]

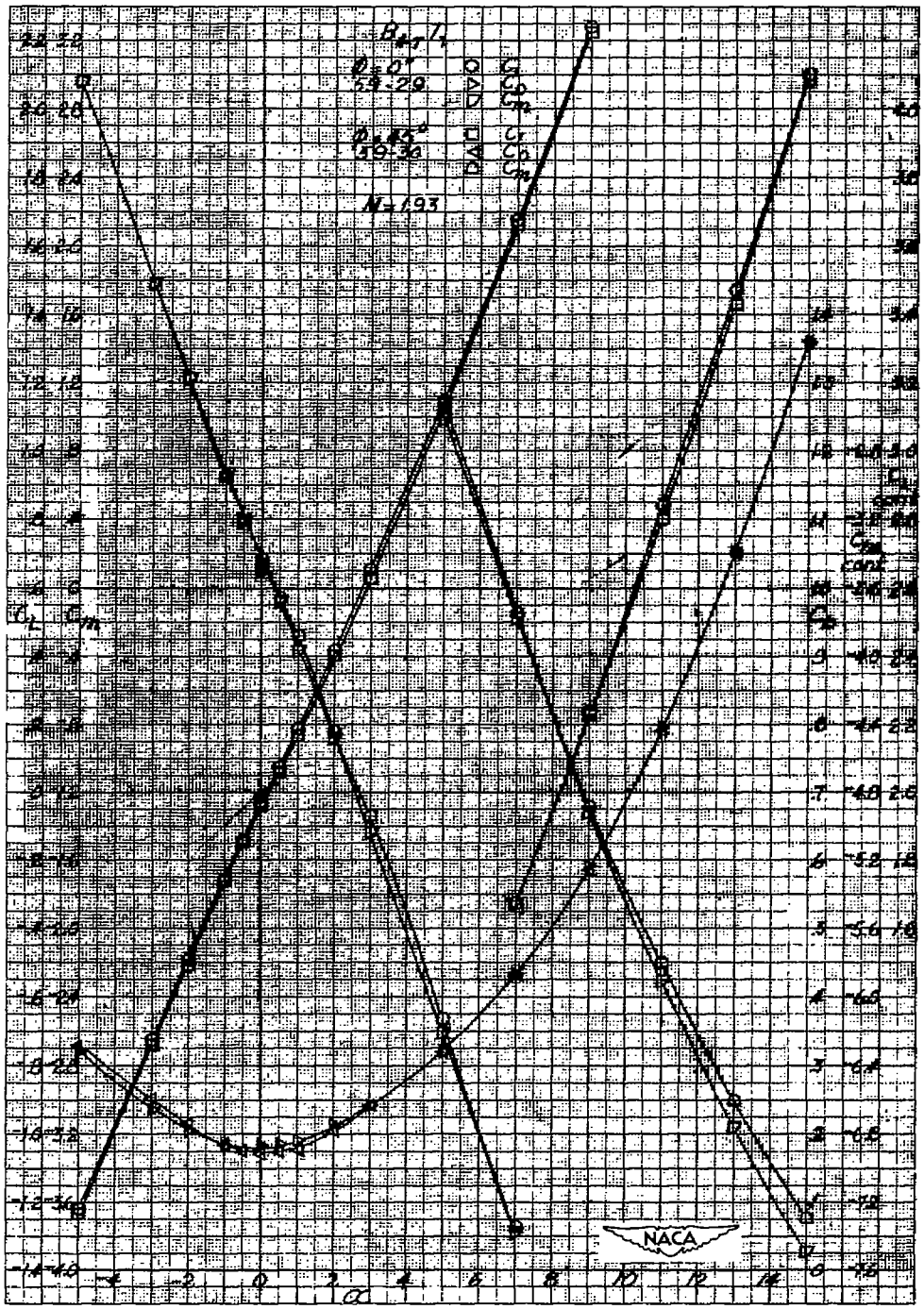

Figure 5.- M = 1.93: T_7 increments on B_{4_T} at roll angles of 0° and 45°.

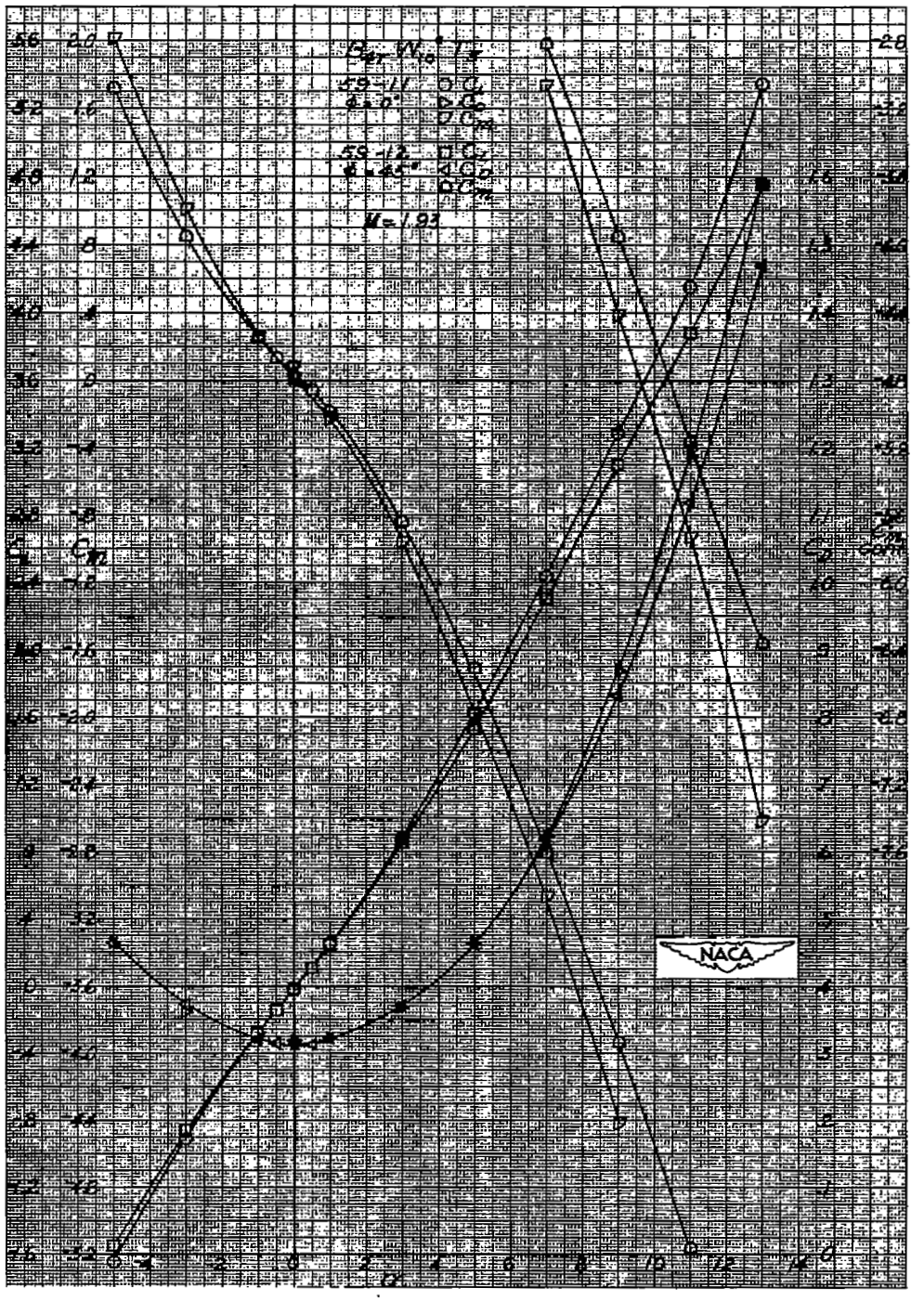

Figure 6.- M = 1.93: Effects of roll position on $B_{4_T}W_{10}{}^{0}T_{5}$; ϕ = 0° and 45°.

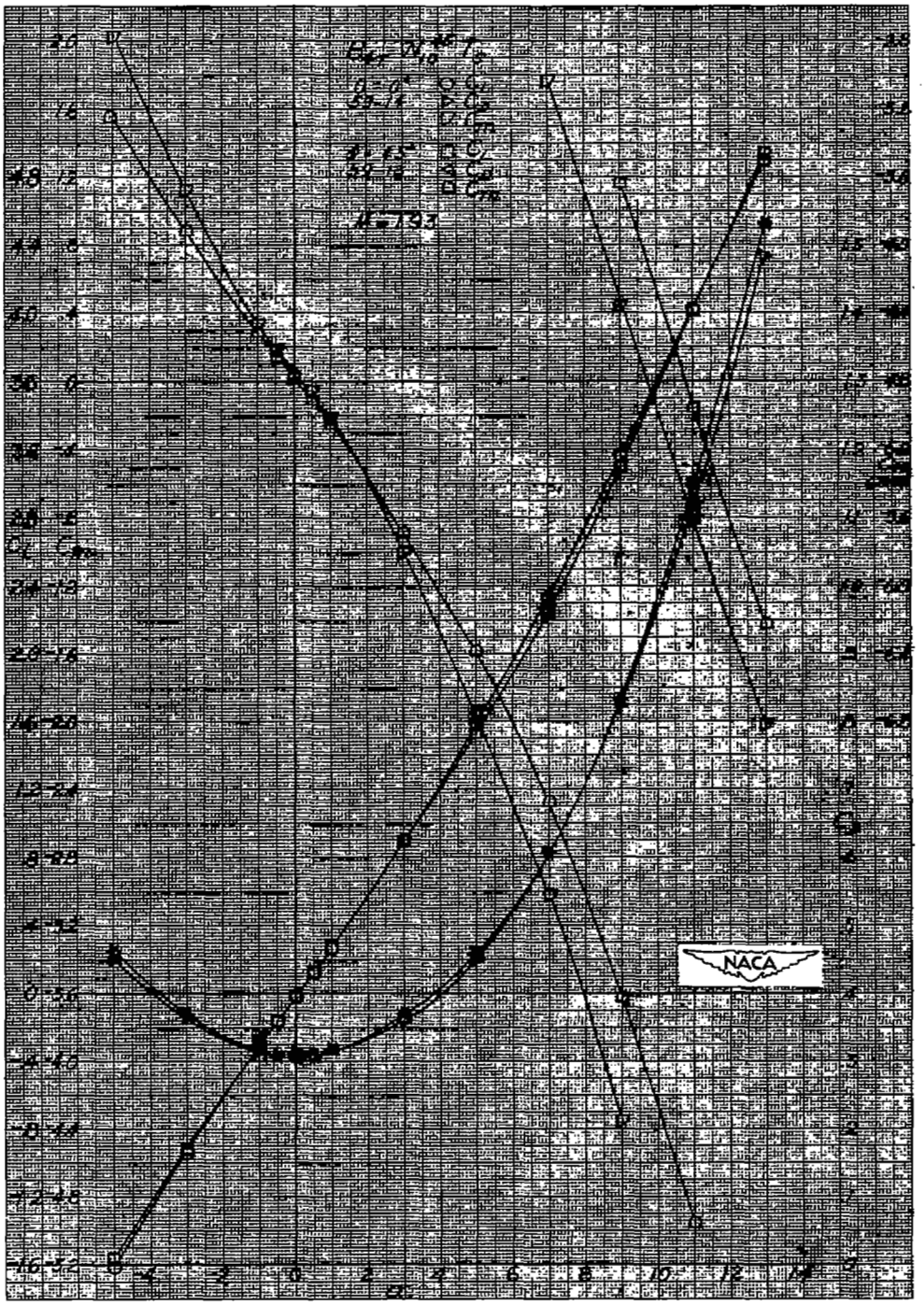

Figure 7.- M = 1.93: Effects of roll position on $B_{4T}W_{10}{}^{45}T_5$; $\phi = 0°$ and 45°.

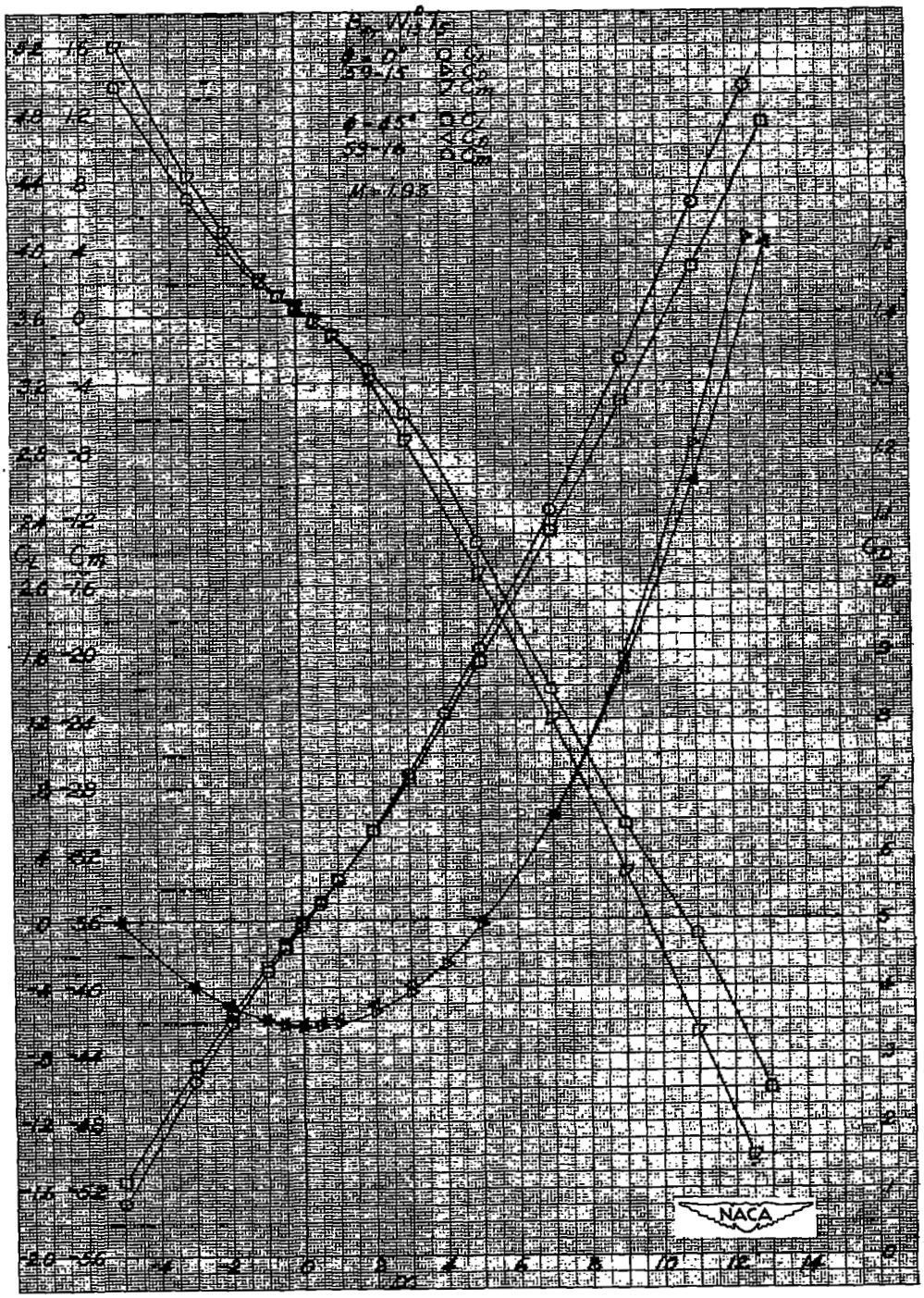

Figure 8.- M = 1.93: Effects of roll position on $B_{4_T}W_{13}{}^{0}T_5$; $\phi = 0°$ and 45°.

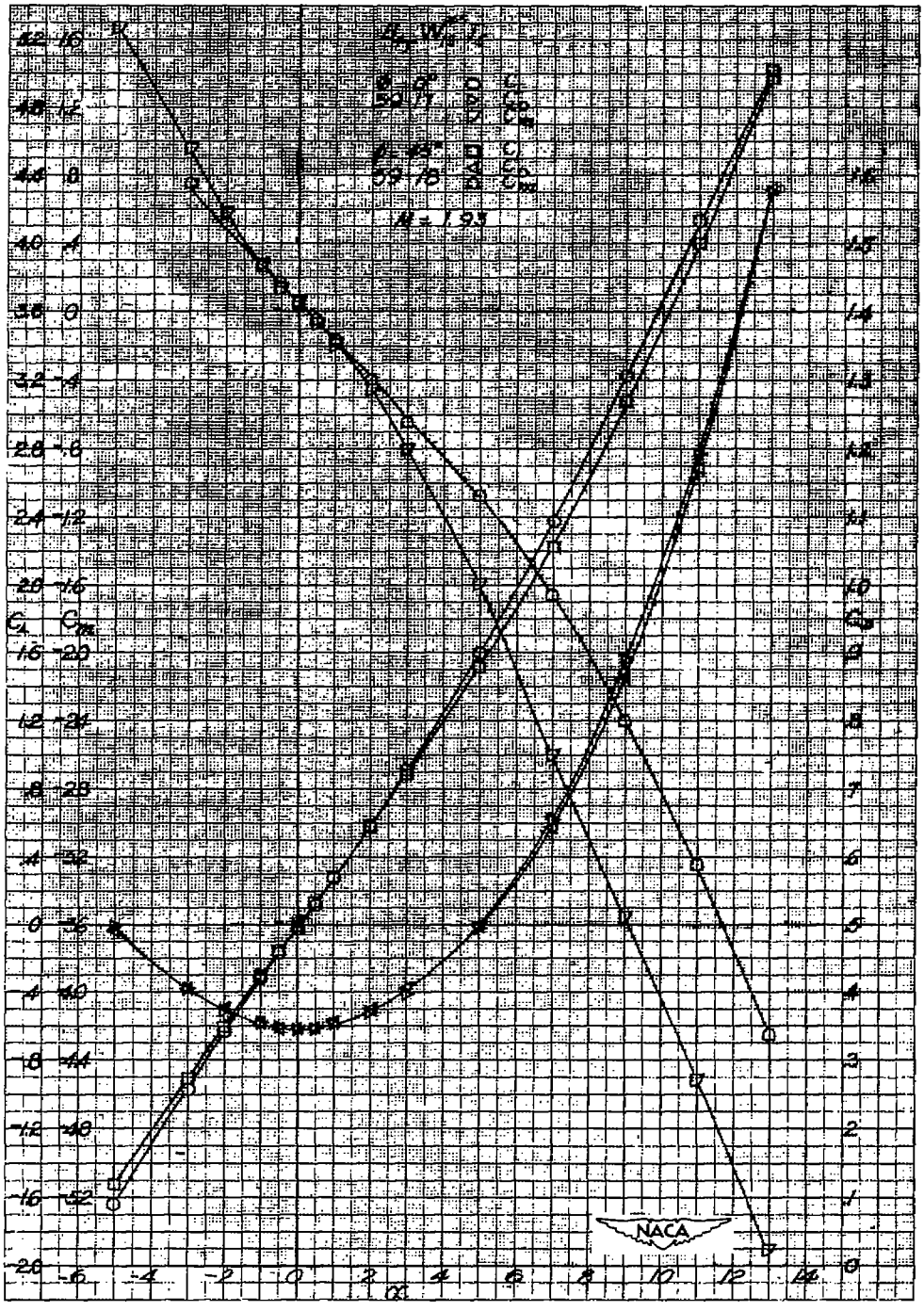

Figure 9.- M = 1.93: Effects of roll position on $B_{4_T}W_{13}{}^{45}T_5$; ϕ = 0° and 45°.

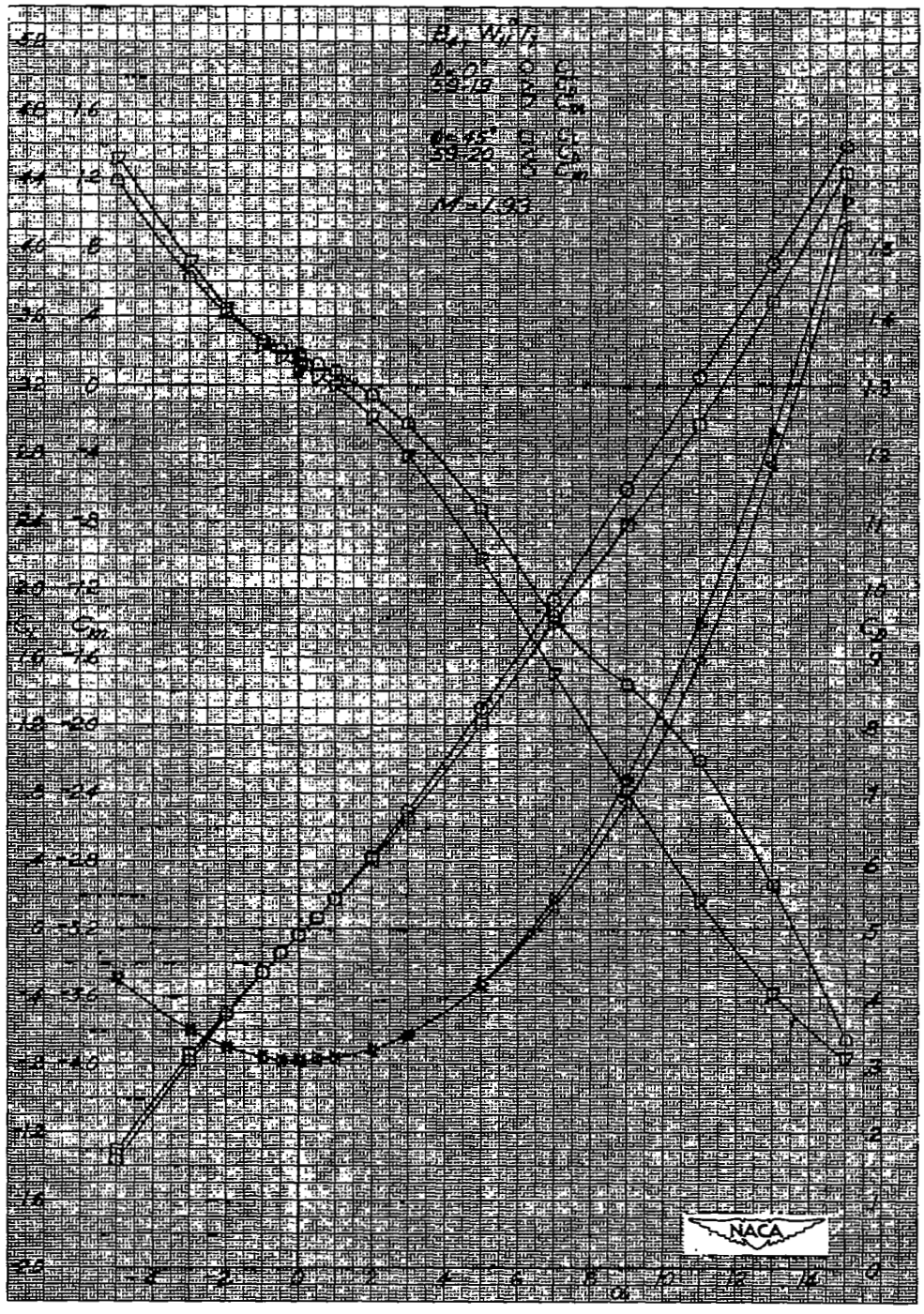

Figure 10.- M = 1.93: Effects of roll position on $B_{4_T}W_{11}{}^{O}T_7$; ϕ = 0° and 45°.

[redacted]

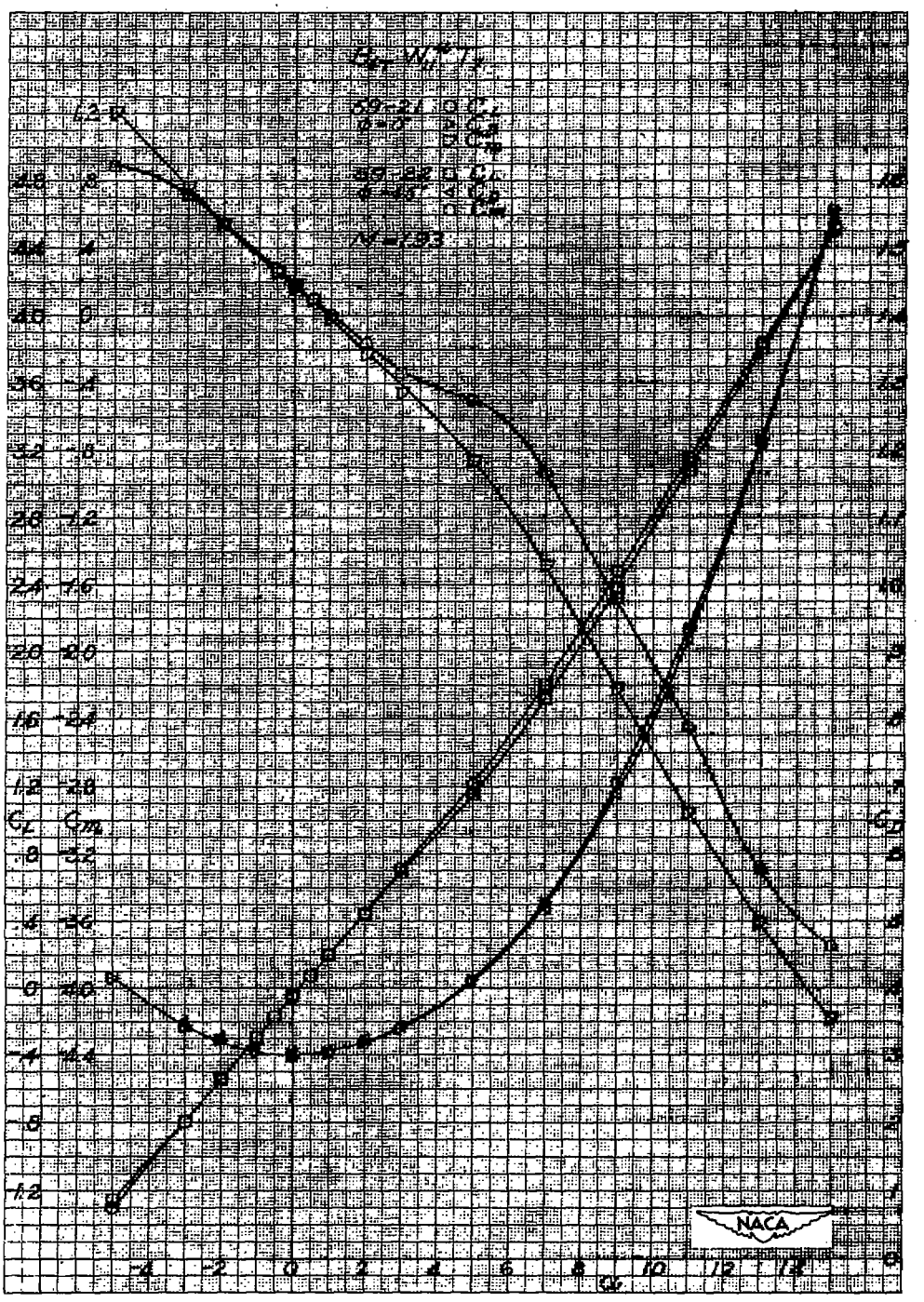

Figure 11.- M = 1.93: Effects of roll position on $B_{4_T}W_{11}{}^{45}T_7$; ϕ = 0° and 45°.

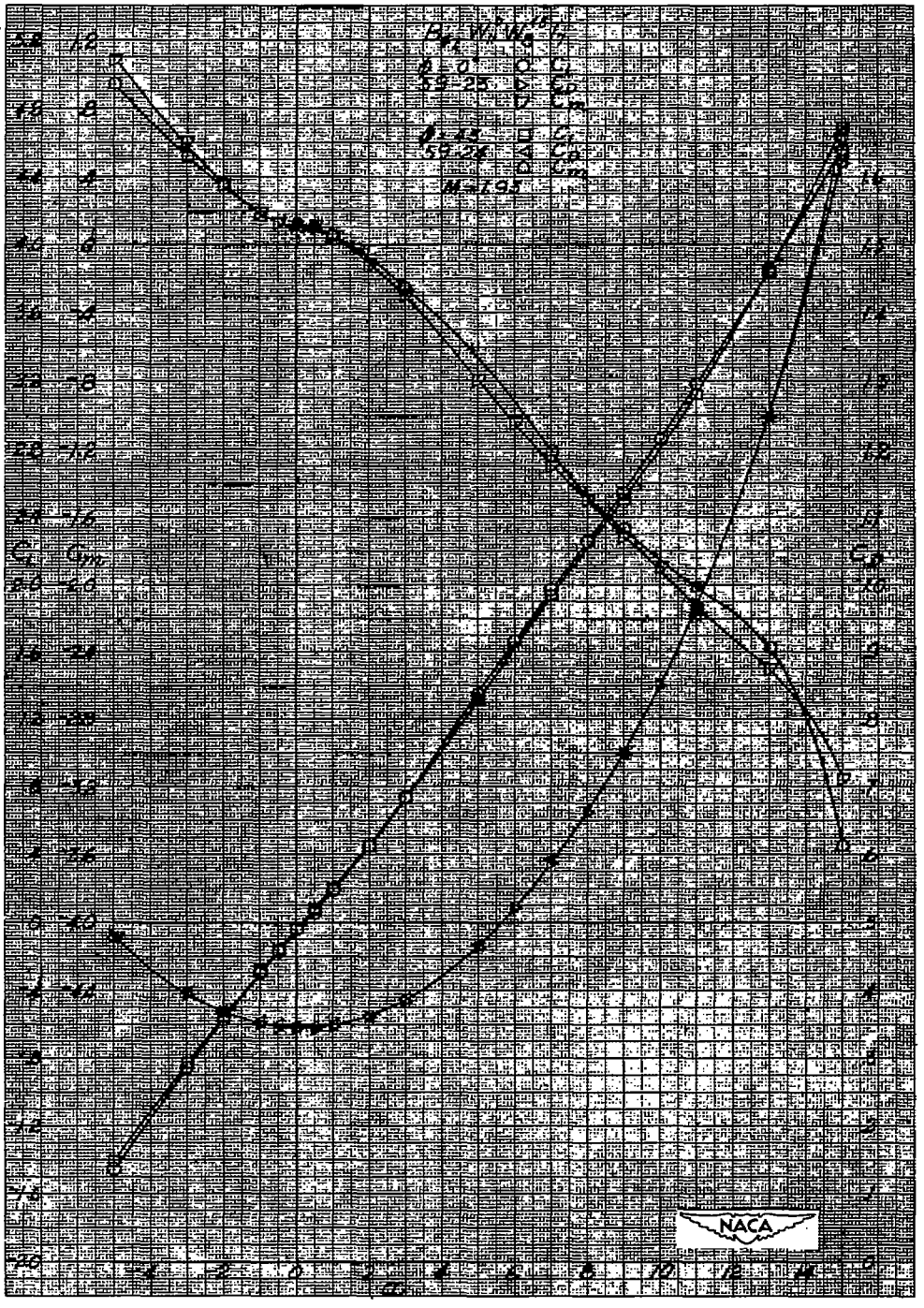

Figure 12.- M = 1.93: Effects of roll position on $B_{4_T}W_{11}{}^{0}W_{8}{}^{45}T_{7}$; $\phi = 0^{\circ}$ and 45°.

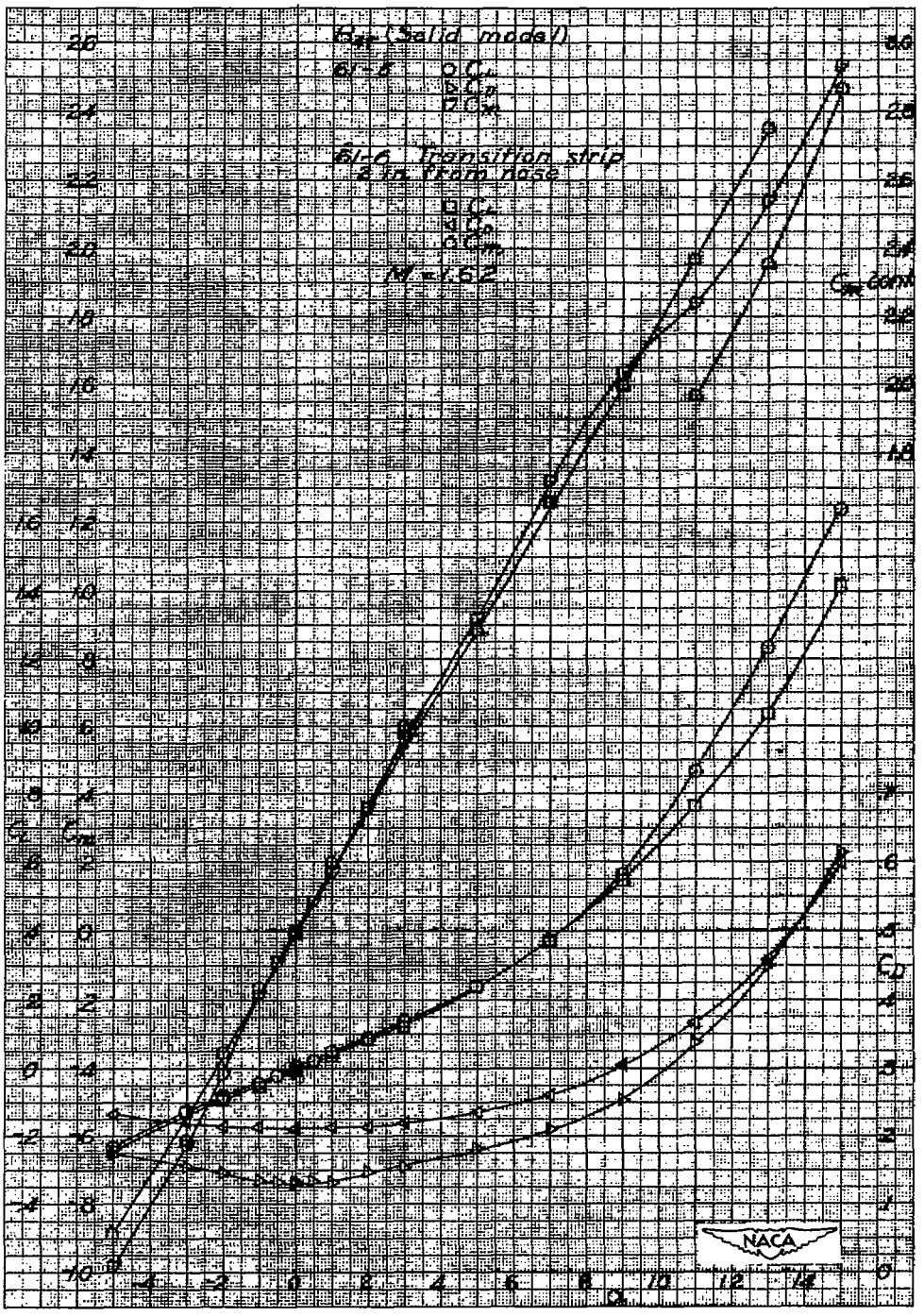

Figure 13.- M = 1.62: Effects of transition on basic solid body characteristics, $B4_T$.

[redacted]

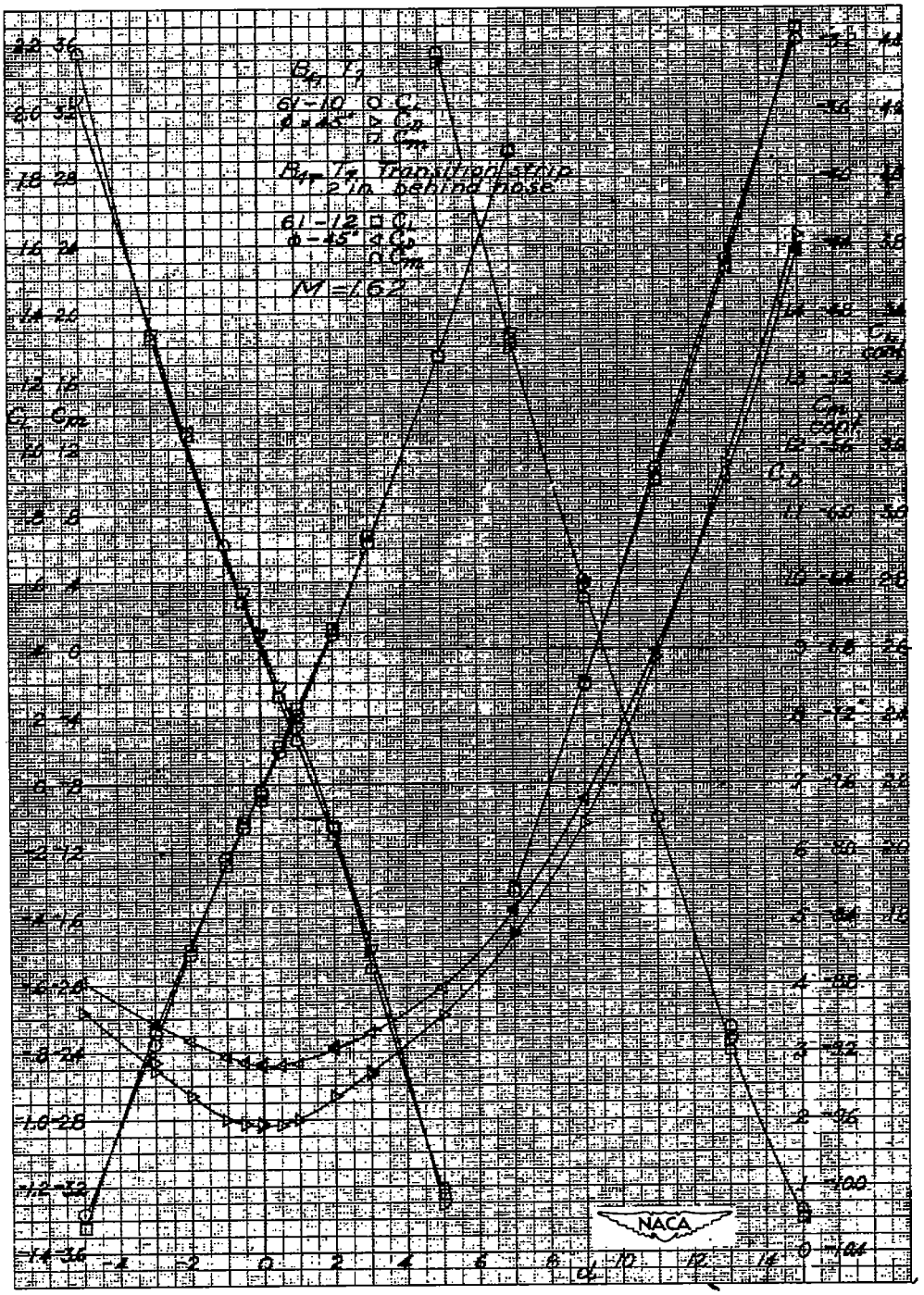

Figure 14.- M = 1.62: T_7 increments on B_{4_T} at a roll angle of 45°.

[redacted]

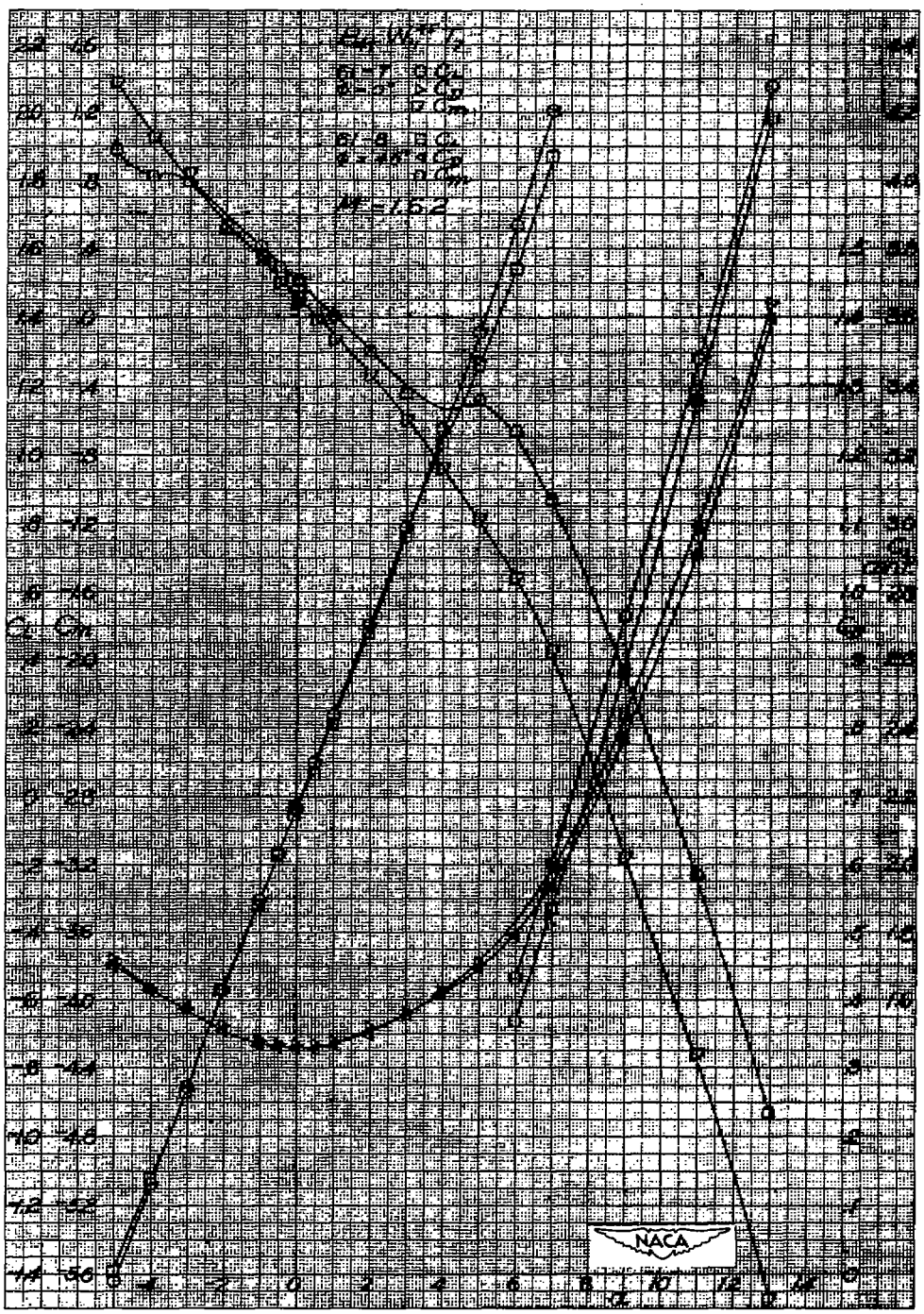

Figure 15.- M = 1.62: Effects of roll position on $B_{4_T}W_{11}{}^{45}T_7$; ϕ = 0° and 45°.

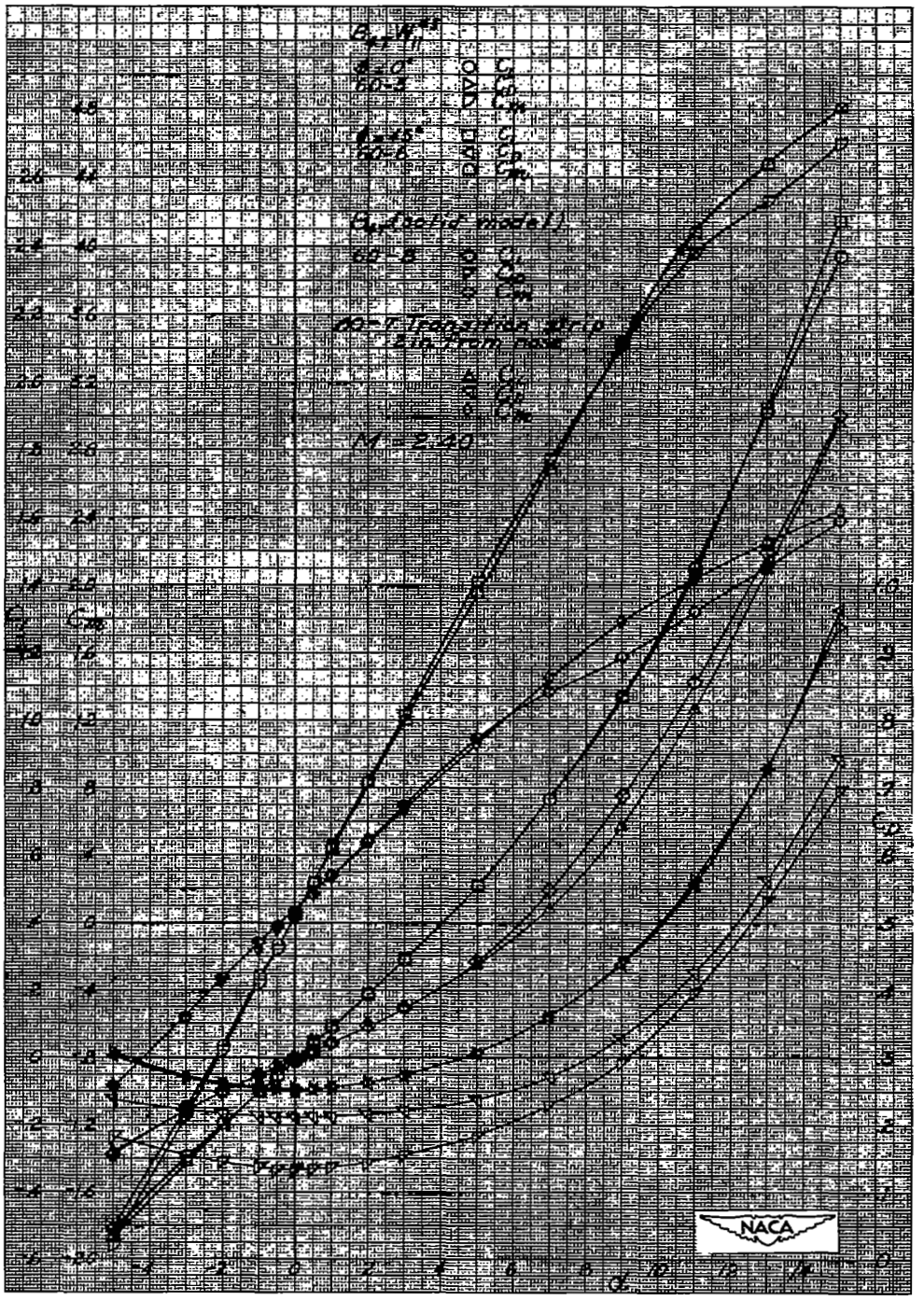

Figure 16.- M = 2.40: Effects of transition on basic solid body characteristics, B_{4_T}; $W_{11}{}^{45}$ increments on B_{4_T} at roll angles of 0° and 45°.

[redacted]

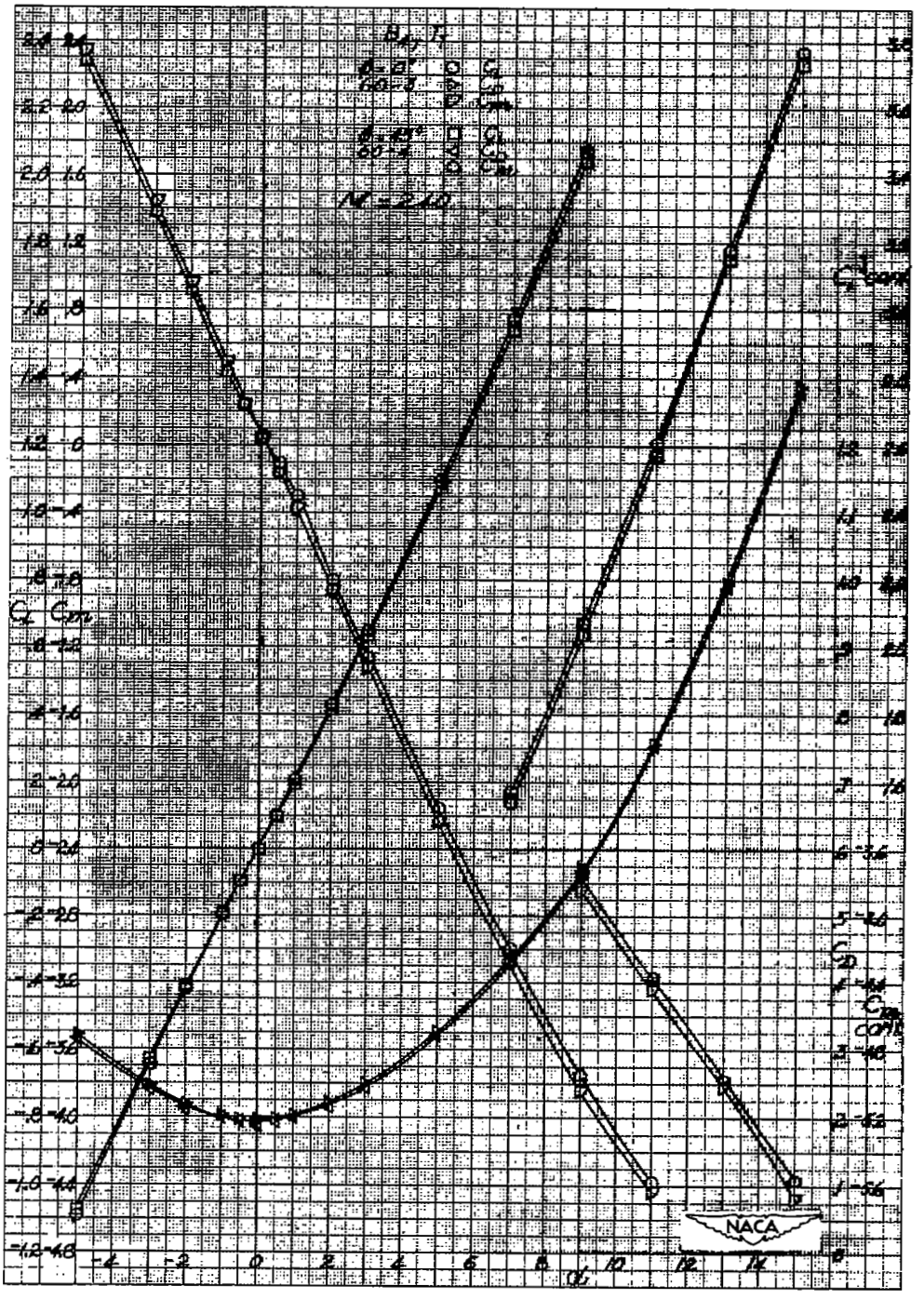

Figure 17.- M = 2.40: T_7 increments on B_{4_T} at roll angles of 0° and 45°.

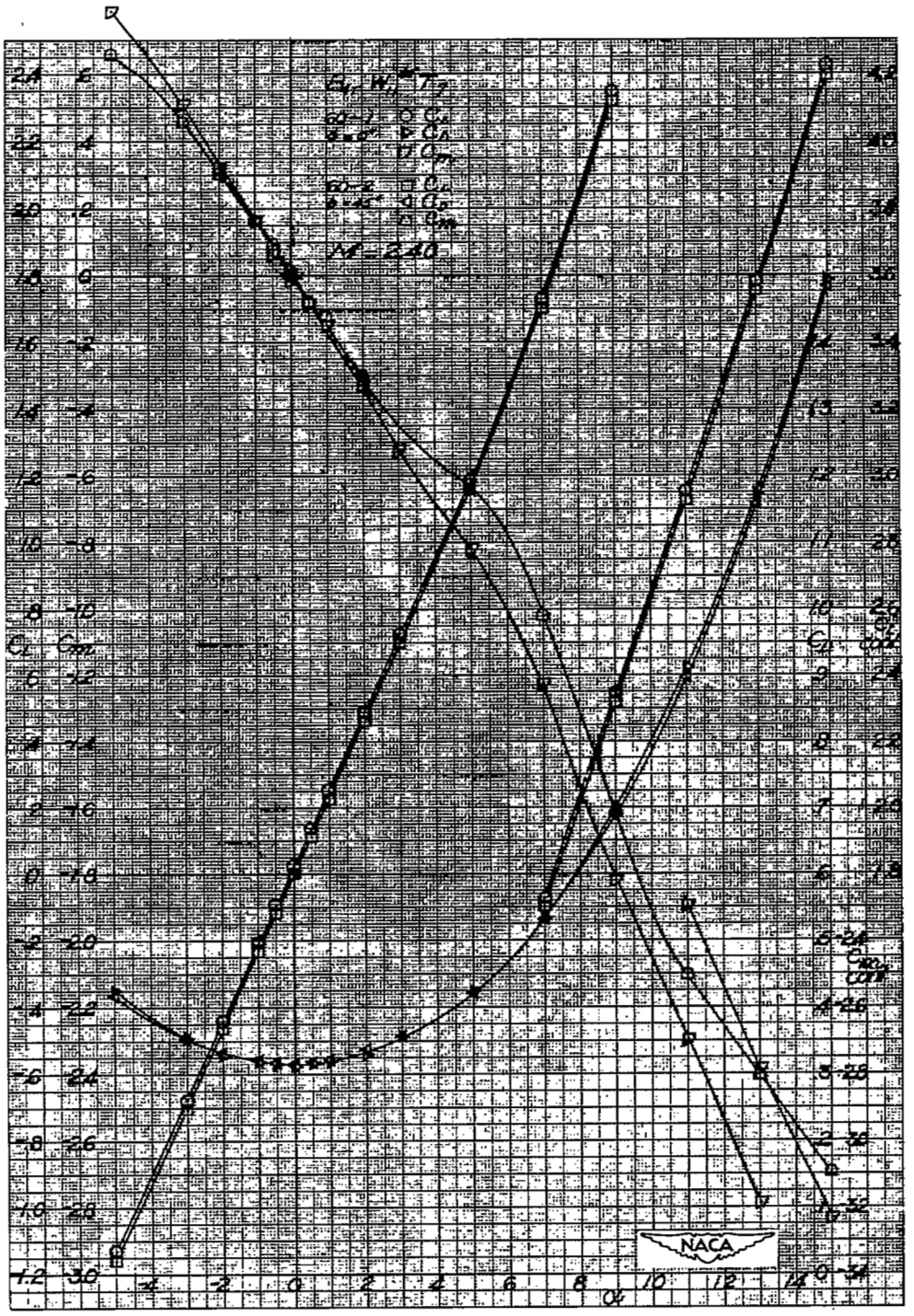

Figure 18.- M = 2.40: Effects of roll position on $B_{4_T}W_{11}{}^{45}T_7$; $\phi = 0^\circ$ and 45°.